Forgery Detection by Internal Positional Learning of Demosaicing Traces

Quentin Bammey, Rafael Grompone von Gioi, Jean-Michel Morel

Forgery Detection by Internal Positional Learning of Demosaicing Traces

Quentin Bammey, Rafael Grompone von Gioi, Jean-Michel Morel
Université Paris-Saclay, ENS Paris-Saclay, CNRS, Centre Borelli

Abstract

We propose 4Point (Forensics with Positional Internal Training), an unsupervised neural network trained to assess the consistency of the image colour mosaic to find forgeries. Positional learning trains the model to learn the modulo-2 position of pixels, leveraging the translation-invariance of CNN to replicate the underlying mosaic and its potential inconsistencies. Internal learning on a single potentially forged image improves adaption and robustness to varied post-processing and counter-forensics measures. This solution beats existing mosaic detection methods, is more robust to various post-processing and counter-forensic artefacts such as JPEG compression, and can exploit traces to which state-of-the-art generic neural networks are blind.

1. Introduction

Image forgeries are omnipresent, from fake news in social networks [53] to scientific misconduct. Indeed, a large variety of image processing tools are available to create visually realistic image alterations. Image forensics aims at detecting and characterizing these alterations. This can be done by analysing traces left behind by the image processing chain, and detecting its local inconsistencies caused by tampering. This analysis is difficult because of the variety of interactions between the successive image processing steps, such as demosaicing, gamma correction, and JPEG encoding. These operations are often complemented by further, equally unknown, post-processing such as resampling and even potential anti-forensic attacks.

The large field of image forensics has been approached in two ways: syntactic analysis and deep learning. The recent deep learning models are directly or indirectly trained to find forgeries in images. ManTraNet [59] is an end-to-end network trained directly on forged images to extract their features and localize inconsistent regions.

Work funded by French *Ministère des Armées – Direction Générale de l'Armement*.

Centre Borelli is also a member of Université Paris Cité, SSA and INSERM.

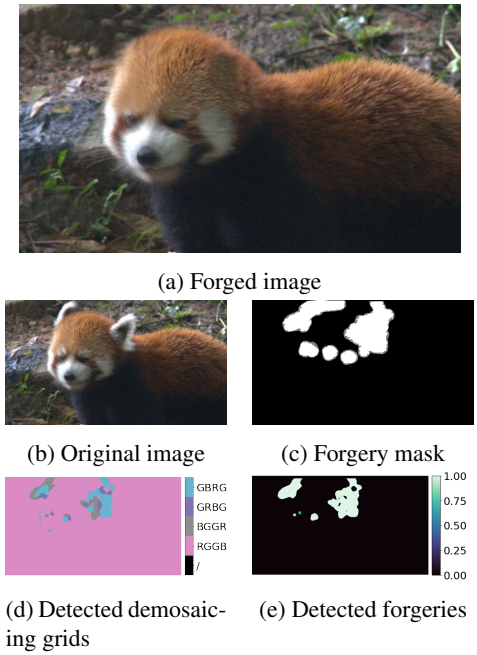

(a) Forged image

(b) Original image

(c) Forgery mask

(d) Detected demosaicing grids

(e) Detected forgeries

Figure 1: Results of the proposed method on an inpainted image from the Korus [36, 37] dataset. Local detection of the demosaicing pattern not only enables detection of the forgery, but also shows the patches used during inpainting.

Noiseprint [14] extracts the noise pattern of the image and finds its inconsistencies by means of Siamese networks. Bappy et al. [6, 7] approach forgery detection as a binary segmentation problem between forged and authentic regions. The Achilles' heel of these methods is the training database itself. Working very well on images and forgeries similar in nature to the database, they may nevertheless fail to adapt to the variety of images and forgery methods.

Syntactic analysis instead focuses on specific inconsistencies left by forgeries. For instance, Error Level Analysis [28] compresses the image and uses the residual between the original and compressed versions to find areas in which compression levels are different. Many methods look for inconsistencies in the traces left by JPEG compression [47, 58, 27, 39, 40, 9, 1] or noise discrepancies [30, 51, 13, 22, 43, 44, 8, 45, 35, 56, 29, 15, 48, 42, 41, 60, 57].

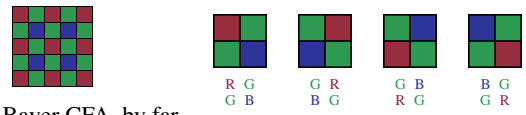

(a) The Bayer CFA, by far the most commonly used CFA.

(b) The four potential patterns that arise from the Bayer CFA.

Figure 2: The Bayer Colour Filter Array (CFA), and the four potential patterns that arise from it. The pattern identifies the offset of the CFA.

However, forgery tools are varied, and so is the plethora of postprocessing operations, both occurring naturally through the treatment and distribution of the image, or maliciously made to hide the forgery. The syntactic methods therefore often miss forgeries that did not modify the statistics of the image in an expected way, or whose traces were erased by further processing. Nevertheless, these methods yield explainable and easily understood results.

One of the classic syntactic methods is to analyse the traces of demosaicing. Most cameras recreate the colour image from a Bayer pattern (shown in Fig. 2a) that samples just one colour channel per pixel. This pattern is 2×2 periodic. Demosaicing is a clever nonlinear interpolation method recreating the two missing colour channels at each pixel from the observed channel values in a neighborhood. Demosaicing algorithms have shown in recent year a growing sophistication, from standard manual methods [26, 49, 20, 21] to complex classic ones [31, 32, 46] and eventually to deep-learning-based [55].

Demosaicing is of interest to image forensics, because when an image is forged by splicing or copy-move, there is a $\frac{3}{4}$ chance that the mosaic patterns of the authentic and forged regions will not be aligned. Being able to detect local inconsistencies of the original mosaic pattern can thus help find such forgeries. Most manual methods [4, 12, 54] easily detect the presence of demosaicing, but fail to detect the position of the mosaic pattern, due to the extreme variety of demosaicing algorithms. Recently, Bammey et al. [3] used deep learning to identify the correct position, even on unseen demosaicing algorithms. However, even recent state-of-the-art methods fail to detect the mosaic pattern of images after common post-processing such as JPEG compression, even at a very high quality factor. Furthermore, post-processing, and especially JPEG compression, can be done in various ways. As a consequence, deep learning-based methods must take into account the impossibility to learn on all existing demosaicing algorithms.

In this article, inspired by [3, 38], we propose a self-supervised learning method that leverages the translation invariance of a CNN to implicitly interpret demosaicing traces. Inconsistencies in the detected traces are then evidence of possible forgeries (see Fig. 1). We borrow from [3] the idea of performing self-supervised learning of the demosaicing grid position. Our method enables internal learning on a single test image, without the need for a large database of similarly-processed images. Using our own JPEG compression in several different alignments further improves robustness to JPEG compression. Furthermore, it becomes able to detect not only regions with a different grid position, but also regions with incoherent grid positions, like those caused by most inpainting methods. The proposed method detects separately the diagonal inconsistencies, that are generally more solid, then detects the general pattern inconsistencies. Last but not least, we process the results of the network to filter out irrelevant results, instead of relying on the often-overconfident [25] raw results of the neural network. Overall, our results are more robust and interpretable.

We show that the CNN can be directly fine-tuned on a single image (internal learning) to assess its consistency, by training on it as if it were authentic, and that this retraining makes the network more robust to various post-processing methods. As a consequence, our network is able to adapt to a broader range of images, even if the network was not initially trained on the same specific post-processing chain.

Because JPEG compression destroys the high frequencies of an image in which demosaicing traces are located, there is no hope to detect them when an image has suffered strong compression or has been downsampled. This means that demosaicing artefact detection is irrelevant to images found, for instance, in social media. Nevertheless, being able to achieve some degree of robustness when the JPEG compression is not too strong can make such methods useful in other many areas, such as criminal investigations, press authentication or photographic contest verification.

To tackle the variety of existing post-processing algorithms and combinations thereof, we show that the network can be fine-tuned on-the-fly on a single, potentially forged, image by training on it as if it was authentic. Adapting to the image's statistics in this way helps the network improve its interpretation of demosaicing traces over common post-processing methods and detect forgeries.

2. Related Works

In a pioneer paper [50], Popescu and Farid proposed to use an expectation-maximization (EM) algorithm to jointly estimate the demosaicing algorithm of an image and detect the local Bayer pattern. A Fourier transform of the resulting pseudo-probability map then shows the presence or absence of demosaicing on the image. The methods in [24, 2] replace the EM algorithm with a direct linear estimation of the algorithm in all four possible positions. The method of [24] further uses the Discrete Fourier Transform (DCT) instead of the FFT, to detect not just the mere presence of demosaicing, but also changes of the mosaic position. Indeed, a change in the sign of the DCT is easier to detect than

a phase change in the FFT. All of these methods assume demosaicing was performed independently in each colour channel and a linear estimation is a valid representation of the demosaicing process. These assumptions are no longer true with most commonly-used demosaicing methods.

Kirchner [34] proposed to directly detect the mosaic position used in the image. To do so, the authors mosaic the image in all four possible positions, and redemosaic it with bilinear interpolation. When this is done in the correct position, the processed image is closer to the original image, enabling detection of the correct pattern. Due to the large variety of demosaicing algorithms, this method does not work well in the wild, but can provide reliable results when the algorithm used by the camera is known or can be estimated.

Choi et al. [12] remarked that interpolated pixels are more likely to take intermediate values than sampled pixels. Counting the number of intermediate values in each of the four patterns thus provides a simple estimate the pattern, although the decision can be confused with modern algorithms that do not process colour channels independently.

Shin [54] uses the fact that most algorithms do not process colour channels, but more or less directly the difference between the green and the other two channels. As a consequence, they work on the difference of channels to find the pattern with the highest variance, which corresponds to a higher probability of being originally sampled, thus breaking free from the assumption of channel independence.

In previous work [3], we trained a self-supervised neural network that detects the relative position modulo 2 of pixels and blocks in the image. Because a CNN is invariant to translation, it implicitly needs to learn from mosaic artefacts in order to perform this classification. Shifts in the output of the network are thus evidence of forged regions. This network can be fine-tuned on a dataset of potentially forged images, which enables it to adapt to it and gain some robustness to JPEG compression.

In recent years, internal learning has gained popularity in several domains of image processing. Using self-supervised information to retrain an over-parameterized network on the very image to process, such methods often provide better results and greater adaptability to uncontrolled cases than their supervised counterparts. For instance, in the close field of image denoising, Noise2Void [38] and the subsequent Self2Self [52] train a network to reconstruct a noisy image while hiding pixels from its input. The network provides the regularization necessary to actually denoise the image.

3. Method

We propose to train a fully-convolutionnal neural network (CNN) to detect the positional information on each pixel of an image. Because a CNN is invariant to translation, it does not know these positions and has to infer them from camera traces, in particular from demosaicing traces.

Figure 3: The four possible sampling patterns can be grouped by the diagonal on which the green channel was sampled: $\begin{smallmatrix}R&G\\G&B\end{smallmatrix}$ and $\begin{smallmatrix}B&G\\G&R\end{smallmatrix}$ share the $\begin{smallmatrix}\cdot&G\\G&\cdot\end{smallmatrix}$ diagonal, whereas $\begin{smallmatrix}G&R\\B&G\end{smallmatrix}$ and $\begin{smallmatrix}G&B\\R&G\end{smallmatrix}$ share the $\begin{smallmatrix}G&\cdot\\\cdot&G\end{smallmatrix}$ one.

Inconsistencies in the output of the network reveal inconsistencies in the demosaicing pattern, and are thus traces of forgeries. In Sec. 3.1, we explain how the network is trained on positional data. In Sec. 3.2, we show how some level of robustness to JPEG compression can be achieved during training. In Sec. 3.3, we show that it is possible to retrain this network directly on a single suspicious image to adapt to the setup of this image, thus achieving a greater robustness to JPEG compression. Finally, in Sec. 3.4, we detail how the network's output can be used to detect forgeries.

3.1. Positional learning

A CNN is invariant to translation; it does not *know* the position of an image's pixels. If we train it to do so, it thus has to rely on external cues, such as demosaicing traces. After such training, the network is thus able to provide an insight as to the image's demosaicing.

Bammey et al. [3] proposed to train a CNN to detect the modulo 2 position of each pixel, both horizontally and vertically. Coarser-scale position information is irrelevant to the very local demosaicing traces, and could lead the network to rely on unwanted cues. However, demosaicing detection algorithms [4, 12, 54, 34] usually proceed in two steps: they start by detecting the diagonal pattern, i.e. to find which pixels were sampled in green, then try to distinguish between the two patterns sharing the same diagonal, because the diagonal is easier and more robust than directly making a decision on the full pattern.

To adopt this, we trained a CNN to detect the offset of each pixel's diagonal (Fig. 4a), representing whether the pixel is sampled in green. For pixels that are not sampled in green, we also estimate whether they are on an even line (Fig. 4b), saying whether they are sampled in red or blue.

This method is self-supervised, since the position of each pixel is known. The only requirement is that all images of the training set be demosaiced in the $\begin{smallmatrix}R&G\\G&B\end{smallmatrix}$ pattern, to enforce consistency of the output across images and correspondence between the detected position and the sampled colour[1]. If a training image has been demosaiced in another pattern, we align it to $\begin{smallmatrix}R&G\\G&B\end{smallmatrix}$ by cropping its first row and/or column.

We use a 17×64 DnCNN [61] architecture, with 17 lay-

[1] If images whose grid is known were not available, it would still be possible to train on images of an unknown grid by applying the same method as during internal learning (see Sec. 3.3).

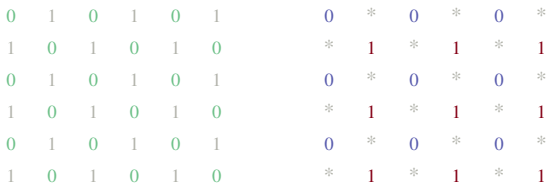

(a) The first detected feature is the diagonal offset. It corresponds to whether the pixel was sampled in green.

(b) The second feature is the evenness of the line/column of the pixel on the main diagonal. It corresponds to whether the pixel was originally sampled in red or in blue.

Figure 4: The CNN is trained to output these two patterns. Asterisks (*) correspond to values that are ignored.

ers and 64 features per layer. DnCNN is more suited to our task than other standard structures, as it does not make use of any downsampling. The downsampling which is found in most CNN structures would remove the high-frequency information in which demosaicing artefacts are located.

3.2. Training on JPEG-compressed images

JPEG compression is a major obstacle to demosaicing detection. The quantization induced during compression quickly removes the highest frequencies of an image, in which demosaicing traces are located. As a consequence, strongly-compressed images keep no demosaicing traces and cannot be detected by our method. Nevertheless, it remains possible to find demosaicing traces on high-quality images, where the compression is minimal. This prompts us to train our network on JPEG-compressed images.

However, JPEG compression aggregates data in 8×8 blocks, imprinting a strong 8-periodic component. JPEG artefacts would thus be enough for the CNN to find the position of all pixels without even looking at demosaicing traces. To prevent the network from doing this and to force it to analyse the demosaicing artefacts over JPEG compression, we start from uncompressed images and compress them ourselves in the four possible alignments between the demosaicing pattern and the JPEG grid, seen in Fig. 5. For each initial image, we have 4 compressed images with different shifts, and the network is trained simultaneously on them. The network can no longer directly analyse and use JPEG compression to find the positions, as the positional cues from JPEG contradict each other across the shifts.

This training scheme assumes that the JPEG grid is consistent across the image, ie. that the compression happened after the forgery. This assumption is reasonable; if the JPEG grid itself is inconsistent, the forgery will be apparent and much easier to detect through JPEG grid analysis [47, 5].

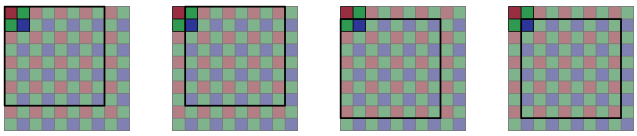

Figure 5: The JPEG grid and the Bayer pattern can be aligned in four different ways. Simultaneous training of the network on the four possible shifts prevents it from using JPEG information instead of the mosaic.

3.3. Internal learning

Training on compressed images already provides some robustness to JPEG compression. However, there is a huge variety of post-processing algorithms, and an even bigger number of combinations thereof, as post-processing encompasses not only algorithms such as JPEG compression, but also image-enhancing filters often automatically applied by cameras, and specific counter-forensic measures such as added noise or median filtering. Furthermore, such algorithms change with time. We propose an alternative strategy. The robustness of our network can be further increased with internal learning, ie. by retraining the network on the specific image we want to study. This enables the network to adapt to the specific statistics of the image.

Given a potentially forged image to analyse, we assume the image is authentic and train the network repeatedly on it to detect the position of pixels, as explained in Sec. 3.1. Contrarily to the initial training, the image is not necessarily in the $\begin{smallmatrix} R & G \\ G & B \end{smallmatrix}$ pattern. To train the network, we compute the loss not only on the initial target of Fig. 4, but we also shift the target by one row and/or column. We thus have 4 losses depending on the offset of the target, we use the one that is minimal across the global image. In other words, we train the network to be locally coherent with the global pattern.

Of course, single-image training induces a risk of overfitting. However, even if the network overfits on the image, training is done on the hypothesis that the full image is authentic. In other words, fine-tuning incentivises the network to conclude that everything is authentic. As a consequence, if the image is actually authentic, the risks of making a false detection are lower than with the pretrained-network; even overfitting will by design not induce new false detections. In the more interesting case where the image is indeed forged, the network will also adapt to the post-processing to learn demosaicing traces and detect the position of pixels. Forged regions in images are usually small compared to the total size. As a consequence, even though the forged regions would steer the network towards detecting their pixels' positions correctly, they would produce evidence contradicting that of much larger authentic regions, and the network should thus not learn too much from forged regions. The small size and locality of the network is particularly impor-

tant here to prevent it from being able to adapt to both, the authentic and the forged regions. The impact of overfitting can thus be expected to be limited.

3.4. Forgery detection

The network does not directly detect forgeries in an image, it only detects pixel-wise, demosaicing-related positional information. This information must then be analysed to find forged regions of an image.

The output of the network consists of two feature maps, following the targets of Fig. 4: the diagonal of the pixel O_d, and the line O_l for pixels on the main diagonal.

These results are aggregated in 2×2 blocks, corresponding to a Bayer CFA tile from fig. 2a. Let B_d and B_l represent a block from O_d and O_l, three binary decisions are made on that block:

- $\delta_{\substack{\cdot & \mathrm{G} \\ \mathrm{G} & \cdot}\,|\,\substack{\mathrm{G} & \cdot \\ \cdot & \mathrm{G}}} \triangleq \left[\frac{1}{4}\left(B_{d_{0,0}} + B_{d_{1,1}} - B_{d_{0,1}} - B_{d_{1,0}}\right)\right]$,
- $\delta_{\substack{\mathrm{R} & \mathrm{G} \\ \mathrm{G} & \mathrm{B}}\,|\,\substack{\mathrm{B} & \mathrm{G} \\ \mathrm{G} & \mathrm{R}}} \triangleq \left[\frac{1}{2}\left(B_{l_{0,0}} - B_{l_{1,1}}\right)\right]$, and
- $\delta_{\substack{\mathrm{G} & \mathrm{R} \\ \mathrm{B} & \mathrm{G}}\,|\,\substack{\mathrm{G} & \mathrm{B} \\ \mathrm{R} & \mathrm{G}}} \triangleq \left[\frac{1}{2}\left(B_{l_{1,0}} - B_{l_{1,0}}\right)\right]$.

In these definitions, $[\cdot]$ represents rounding to 0 or 1. $\delta_{\substack{\cdot & \mathrm{G} \\ \mathrm{G} & \cdot}\,|\,\substack{\mathrm{G} & \cdot \\ \cdot & \mathrm{G}}}$ says in which diagonal the block – or rather its top-left pixel – is detected, from which the pattern diagonal can be inferred: a value of 0 (resp. 1) means the block is demosaiced in a $\substack{\cdot & \mathrm{G} \\ \mathrm{G} & \cdot}$ (resp. $\substack{\mathrm{G} & \cdot \\ \cdot & \mathrm{G}}$) pattern. Assuming we know the block is demosaiced in one of the two $\substack{\cdot & \mathrm{G} \\ \mathrm{G} & \cdot}$ patterns, $\delta_{\substack{\mathrm{R} & \mathrm{G} \\ \mathrm{G} & \mathrm{B}}\,|\,\substack{\mathrm{B} & \mathrm{G} \\ \mathrm{G} & \mathrm{R}}}$ then distinguishes them; a value of 0 (resp. 1) means the block is demosaiced in the $\substack{\mathrm{R} & \mathrm{G} \\ \mathrm{G} & \mathrm{B}}$ (resp. $\substack{\mathrm{B} & \mathrm{G} \\ \mathrm{G} & \mathrm{R}}$) pattern. Similarly, a value of 0 (resp. 1) for $\delta_{\substack{\mathrm{G} & \mathrm{R} \\ \mathrm{B} & \mathrm{G}}\,|\,\substack{\mathrm{G} & \mathrm{B} \\ \mathrm{R} & \mathrm{G}}}$ means the block is demosaiced in the $\substack{\mathrm{G} & \mathrm{R} \\ \mathrm{B} & \mathrm{G}}$ (resp. $\substack{\mathrm{G} & \mathrm{B} \\ \mathrm{R} & \mathrm{G}}$) pattern, assuming we know the block is demosaiced in a $\substack{\mathrm{G} & \cdot \\ \cdot & \mathrm{G}}$ pattern.

Using these blocks, we determine the pattern of the global image. The main diagonal pattern G_D is the mode of $\delta_{\substack{\cdot & \mathrm{G} \\ \mathrm{G} & \cdot}\,|\,\substack{\mathrm{G} & \cdot \\ \cdot & \mathrm{G}}}$ across the whole image ($\substack{\cdot & \mathrm{G} \\ \mathrm{G} & \cdot}$ or $\substack{\mathrm{G} & \cdot \\ \cdot & \mathrm{G}}$). The full pattern G_P is then the mode of either $\delta_{\substack{\mathrm{R} & \mathrm{G} \\ \mathrm{G} & \mathrm{B}}\,|\,\substack{\mathrm{B} & \mathrm{G} \\ \mathrm{G} & \mathrm{R}}}$ or $\delta_{\substack{\mathrm{G} & \mathrm{R} \\ \mathrm{B} & \mathrm{G}}\,|\,\substack{\mathrm{G} & \mathrm{B} \\ \mathrm{R} & \mathrm{G}}}$.

At this stage, we can already have a first estimation of inconsistent regions in an image, by considering a block forged if its detected pattern is different from that of the full image. However, such results are not stable enough. We instead propose to aggregate the blocks in overlapping windows of $W \times W$ blocks, or $2W \times 2W$ pixels. For each window, we define $\Delta_{\substack{\cdot & \mathrm{G} \\ \mathrm{G} & \cdot}\,|\,\substack{\mathrm{G} & \cdot \\ \cdot & \mathrm{G}}}$ (resp. $\Delta_{\substack{\mathrm{R} & \mathrm{G} \\ \mathrm{G} & \mathrm{B}}\,|\,\substack{\mathrm{B} & \mathrm{G} \\ \mathrm{G} & \mathrm{R}}}$, $\Delta_{\substack{\mathrm{G} & \mathrm{R} \\ \mathrm{B} & \mathrm{G}}\,|\,\substack{\mathrm{G} & \mathrm{B} \\ \mathrm{R} & \mathrm{G}}}$) as the mean of $\delta_{\substack{\cdot & \mathrm{G} \\ \mathrm{G} & \cdot}\,|\,\substack{\mathrm{G} & \cdot \\ \cdot & \mathrm{G}}}$ (resp. $\delta_{\substack{\mathrm{R} & \mathrm{G} \\ \mathrm{G} & \mathrm{B}}\,|\,\substack{\mathrm{B} & \mathrm{G} \\ \mathrm{G} & \mathrm{R}}}$, $\delta_{\substack{\mathrm{G} & \mathrm{R} \\ \mathrm{B} & \mathrm{G}}\,|\,\substack{\mathrm{G} & \mathrm{B} \\ \mathrm{R} & \mathrm{G}}}$) across the window. The detected diagonal pattern of the window is

$$D \triangleq \begin{cases} \substack{\cdot & \mathrm{G} \\ \mathrm{G} & \cdot} & \Delta_{\substack{\cdot & \mathrm{G} \\ \mathrm{G} & \cdot}\,|\,\substack{\mathrm{G} & \cdot \\ \cdot & \mathrm{G}}} < \frac{1}{2} \\ \substack{\mathrm{G} & \cdot \\ \cdot & \mathrm{G}} & \text{otherwise} \end{cases}, \tag{1}$$

the demosaicing pattern is then detected as:

$$P \triangleq \begin{cases} \substack{\mathrm{R} & \mathrm{G} \\ \mathrm{G} & \mathrm{B}} & D = \substack{\cdot & \mathrm{G} \\ \mathrm{G} & \cdot} \text{ and } \Delta_{\substack{\mathrm{R} & \mathrm{G} \\ \mathrm{G} & \mathrm{B}}\,|\,\substack{\mathrm{B} & \mathrm{G} \\ \mathrm{G} & \mathrm{R}}} \leq \frac{1}{2} \\ \substack{\mathrm{B} & \mathrm{G} \\ \mathrm{G} & \mathrm{R}} & D = \substack{\cdot & \mathrm{G} \\ \mathrm{G} & \cdot} \text{ and } \Delta_{\substack{\mathrm{R} & \mathrm{G} \\ \mathrm{G} & \mathrm{B}}\,|\,\substack{\mathrm{B} & \mathrm{G} \\ \mathrm{G} & \mathrm{R}}} > \frac{1}{2} \\ \substack{\mathrm{G} & \mathrm{R} \\ \mathrm{B} & \mathrm{G}} & D = \substack{\mathrm{G} & \cdot \\ \cdot & \mathrm{G}} \text{ and } \Delta_{\substack{\mathrm{G} & \mathrm{R} \\ \mathrm{B} & \mathrm{G}}\,|\,\substack{\mathrm{G} & \mathrm{B} \\ \mathrm{R} & \mathrm{G}}} \leq \frac{1}{2} \\ \substack{\mathrm{G} & \mathrm{B} \\ \mathrm{R} & \mathrm{G}} & D = \substack{\mathrm{G} & \cdot \\ \cdot & \mathrm{G}} \text{ and } \Delta_{\substack{\mathrm{G} & \mathrm{R} \\ \mathrm{B} & \mathrm{G}}\,|\,\substack{\mathrm{G} & \mathrm{B} \\ \mathrm{R} & \mathrm{G}}} > \frac{1}{2} \end{cases}. \tag{2}$$

We can now introduce a forgery detection confidence score to windows. Windows that are detected in the same grid than the original image, i.e. where $P = G_P$, are given a zero confidence; they are considered authentic. Windows whose detected diagonal is different than the original image's, i.e. where $D \neq G_D$, are given an initial confidence of $2 \cdot \left|\Delta_{\substack{\cdot & \mathrm{G} \\ \mathrm{G} & \cdot}\,|\,\substack{\mathrm{G} & \cdot \\ \cdot & \mathrm{G}}} - \frac{1}{2}\right|$. If a region is detected with high confidence as forged, nearby regions that may be detected with a lower confidence are likely to be part of the forgery as well. Consequently, we segment the detected windows into connected components. Two inconsistent windows are connected iff they can be joined by a path of windows of the same diagonal. The detection confidence of all the windows in this component is then set to the value of the most confident of those windows.

Likewise, windows whose detected diagonal is consistent, but whose pattern is not, i.e. where $D = G_D$ but $P \neq G_P$, are given an initial confidence of $2 \cdot |\Delta - \frac{1}{2}|$, where Δ is either $\Delta_{\substack{\mathrm{R} & \mathrm{G} \\ \mathrm{G} & \mathrm{B}}\,|\,\substack{\mathrm{B} & \mathrm{G} \\ \mathrm{G} & \mathrm{R}}}$ or $\Delta_{\substack{\mathrm{G} & \mathrm{R} \\ \mathrm{B} & \mathrm{G}}\,|\,\substack{\mathrm{G} & \mathrm{B} \\ \mathrm{R} & \mathrm{G}}}$ depending on the diagonal. Segmentation in connected components of the same grid and component-wise maximum are applied as above.

4. Experiments

4.1. Experiments setup

To train our network, we used the 1488 raw images from the Dresden database [23] and demosaiced them with several demosaicing methods: AICC [16, 17], RI [31], MLRI [32], ARI [46], CDMCNN [55, 18], CS [21], GBTF [49], Alternating Projections [19], HA [26], LMMSE [20] and bilinear demosaicing. Training was done with Adam [33] with a learning rate of 10^{-3}. During internal training on each image, the network was retrained for 15 iterations.

Experiments were done on two datasets. The Korus [36, 37] database contains 220 high-quality splicing forgeries, on images from 4 different cameras. The Trace [5] database introduces invisible forgery traces in the form of pipeline inconsistencies. Each raw image is processed with two different camera pipelines, then both obtained images are merged according to a forgery mask. The content of the image stays unchanged, only the pipeline is altered. The database is divided into several datasets with the same images and masks but different changes in the pipeline. Two of these are of particular interest to us; the CFA grid dataset, in which the forged region is demosaiced in a different pattern; and the

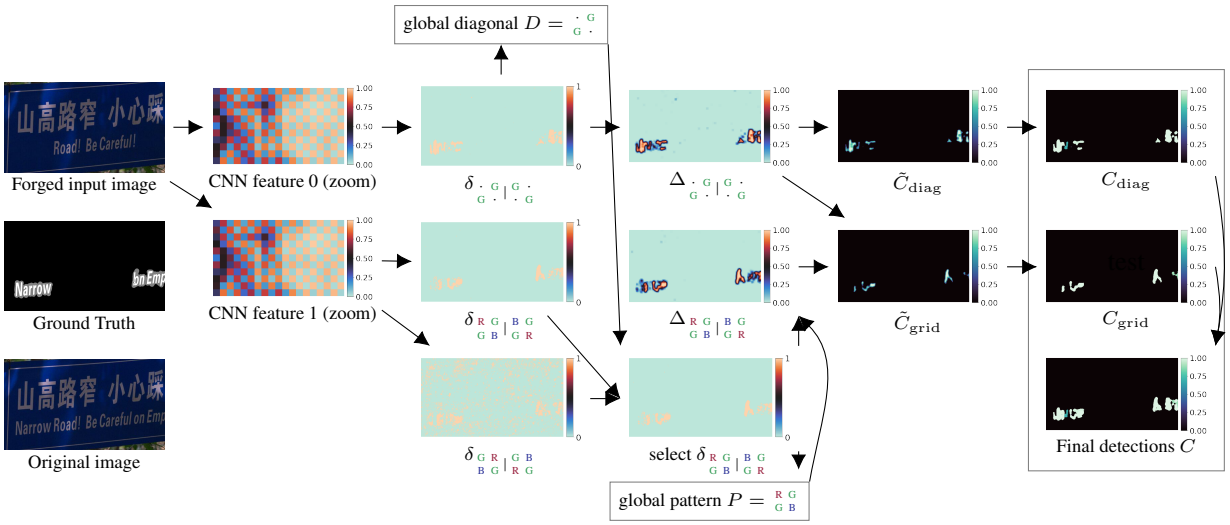

Figure 6: From the output of the network to forgery detection. First, the diagonal is detected in each 2×2 block, then aggregated on overlapping windows. The density of block votes for the wrong diagonal provides an initial confidence in forgery detections $\tilde{C}_{diag}$. The confidence map is segmented into connected components, and each component is given the score of its best window, yielding the diagonal forgery confidence map C_{diag}. Then, using the second feature map output of the network, a similar process is repeated with the vote between the two patterns sharing the globally detected diagonal. The grid forgery confidence map C_{grid} is obtained by finding windows that are in the correct diagonal, but with the wrong full pattern. Finally, the final detection map C is the combination of the two maps C_{diag} and C_{grid}.

CFA algorithm, in which the forged region is demosaiced with a different algorithm, and a new demosaicing pattern is selected, which thus has a $\frac{3}{4}$ chance to be different from the authentic region. For each image and dataset, two forgeries are available, using the same pipeline but different masks, one taken from the image segmentation (endomask) and the other from another image (exomask). As our method only detects pattern shifts, we cannot expect to make detections in regions where the demosaicing pattern is the same, i.e. in one quarter of the images of the CFA algorithm dataset. However, since our method is not content-aware, results between the endomask and exomask should be similar. On the CFA grid dataset, we further study our robustness to JPEG compression, by compressing all images before testing.

We compare our method with the state-of-the-art NN-based Noiseprint [14], as well as demosaicing detection tools Bammey [3], Choi [12] (implementation of [4]) and Shin [54]. All methods, including ours, except Noiseprint operate on windows; we set their size to 32×32 pixels.

4.2. Results

Results are presented in Tab. 1 with the Matthews Correlation Coefficient (MCC), which is the cross-correlation coefficient between the ground truth and the detection. This metric, considered the most representative number for detection evaluation [10, 11], varies between -1 and 1, with 1 representing a perfect detection, -1 its complementary. Any random method has an expected score of 0. As all the tested methods produce heatmaps and not binary outputs, the test was done using the best threshold over each dataset.

On the Trace datasets, the method beats the state-of-the-art at all the tested compression levels. The results are similar to Bammey [3] on the uncompressed images, but our method presents a stronger robustness to JPEG compression. Choi [4, 12] presents some robustness to compression as well. Both Bammey and Shin [54] are unable to make any detection on compressed images. Noiseprint [14] is entirely blind to demosaicing pattern shifts, as seen in the Trace CFA Grid datasets. However, its positive results on the CFA Algorithm datasets mean that it is, to some extent, able to detect changes in the demosaicing algorithm used.

On the Korus dataset, our method presents the best results overall, despite images from the Canon 60D dataset presenting no demosaicing artefacts, as also evidenced by the other demosaicing detection methods. This may be due to an absence of any demosaicing or to a downsampling of the images – images are at a lower resolution than the camera's maximal resolution. On the two Nikon cameras, we get MCC scores of 0.412 (Nikon D7000) and 0.408 (Nikon D90). The best score is reached on the Sony α57 camera, where the MCC is 0.628. All demosaicing detection methods perform best on that camera, which is probably due to a demosaicing that leaves more artefacts. Noiseprint is the only method able to provide relevant detections on the

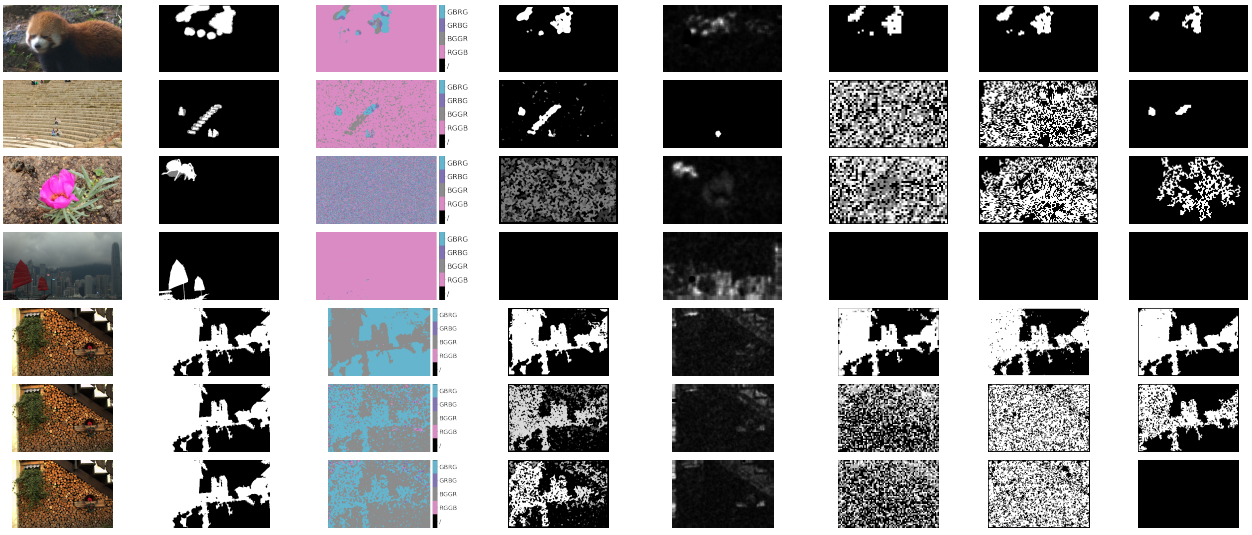

Figure 7: Results on several images from the Korus [36, 37] (first 4 images) and Trace [5] CFA Grid (last 3 images) databases. From left to right: Forged image, forgery mask, detected demosaicing grids with the proposed methods, detected forgeries with the proposed method, and results of Noiseprint [14], Bammey [3], Shin [54] and Choi [4, 12]. As seen on the 1st and 2nd images, detecting the grid enables one not only to find forgeries, but also to precisely know how the forgery (here, an inpainting) was done, by localizing patches with different pattern alignments. On the 3rd image, no demosaicing traces are detected by any method. Still, the forgery can be detected by Noiseprint, which relies on different cues. On the 4th image, the same grid is detected on the whole image; the forged region cannot be detected by demosaicing analysis because the forged region's pattern is aligned. On the last three rows, the same image has been processed uncompressed and at JPEG compression qualities 95 and 90. Even after compression, we can still detect the forgery.

Method	Grid Exo	Grid Endo	Alg Exo	Alg Endo
Proposed	**0.709**	**0.703**	**0.523**	**0.519**
Bammey[3]	0.682	0.665	0.501	0.491
Shin[54]	0.104	0.099	0.085	0.084
Choi[4, 12]	0.603	0.575	0.420	0.385
Noiseprint[14]	-0.001	0.002	0.066	0.060

(a) Results on the CFA Grid (Grid) and CFA Algorithm (Alg) datasets of the Trace [5] database, with endomasks (Endo) and exomasks (Exo)

	UNC	J95	J90
Bilinear	0.732	0.400	0.200
AHD	0.719	0.281	0.123
AAHD	0.680	0.233	0.139
DCB	0.764	0.307	0.132
DHT	0.689	0.193	0.087
PPG	0.714	0.250	0.123
VNG	0.679	0.482	0.252

(b) Results of the proposed method on Trace CFA Grid Exo [5] depending on the demosaicing, on uncompressed (UNC) and compressed (J95, J90) images.

Method	UNC	J95	J90
Proposed	**0.709**	**0.307**	**0.151**
Bammey[3]	0.682	0.005	0.003
Shin[54]	0.104	0.001	0.001
Choi[4, 12]	0.603	0.156	0.070
Noiseprint[14]	-0.001	0.004	0.001

(c) Compared robustness to JPEG compression on Trace CFA Grid exo. UNC means no compression.

Method	Canon 60D	Nikon D7000	Nikon D90	Sony α57	All
Proposed	0.009	**0.401**	**0.378**	**0.624**	**0.353**
Bammey	0.002	0.049	0.044	0.574	0.167
Noiseprint	**0.153**	0.322	0.236	0.148	0.202
Choi	0.004	0.176	0.251	0.251	0.238
Shin	0.021	0.003	0.012	0.511	0.143

(d) Results on the Korus dataset.

Table 1: Compared results on the Trace [5] and Korus [36, 37] datasets, using the MCC metric.

Canon 60D cameras. Although its final score is lower than the proposed method's, we want to highlight that these two methods should be seen as complementary, not as competitors. As seen on the Trace database, Noiseprint is blind to shifts in the demosaicing pattern. Its detections on the Korus datasets are thus based on other kinds of artefacts. On the other hand, the proposed method focuses solely on demosaicing pattern shifts. Both thus provide a different and complementary insight into potential forgeries.

Visual results on different images can be seen on Fig. 7.

4.3. Ablation Study

We test the ability of the proposed method to detect forgeries when its key components are removed in Tab. 2. Although retraining is not strictly needed to analyse images, it improves the robustness of the network to various post-demosaicing processing (Korus) and JPEG compression (Trace). When the results are already clear without retraining, however, the difference is much more minor (uncompressed Trace). Unsurprisingly, pretraining the network on JPEG-compressed images is not necessary when analysing uncompressed images. By forcing the network to diversify its analysis, results are actually slightly lower on uncompressed datasets. Even on compressed images, the network that was not pretrained on JPEG images is still able to adapt to the compression to some extent. Nevertheless, the JPEG-pretrained network we propose is almost as good on uncompressed images, and much better when analysing compressed images. Unless one is certain the images were not compressed, the JPEG-pretrained network is thus better overall. Both JPEG pretraining and internal learning improve robustness to JPEG compression, and best results are achieved when both are used. Without at least one of them, however, the network is unable to make any detections on compressed images. In any case, when JPEG pretraining is performed, it must be done with the shifting strategy presented in Sec. 3.2. Otherwise, the network can be led to directly detect the JPEG pattern instead of detecting the mosaic over the JPEG compression, and its scores are worse than even the network without JPEG pretraining. The loss must also be computed on the four possible offset targets, and back-propagation must be performed on the best one globally. Without this, the network is forced to shift its detections into assuming the image is in the $\begin{smallmatrix}R&G\\G&B\end{smallmatrix}$ pattern, thus harming the results if this is not the case.

Discarding the diagonal pattern detection and only looking at the full patterns lowers the scores. Two thirds of the detectable inconsistencies feature different grids and the same diagonal, yet the diagonal is much easier to identify on more difficult (e.g. compressed) images or smaller inconsistencies, where a diagonal shift is often the only thing that can be detected significantly.

Method	Korus	Trace	Trace J95	Trace J90
Proposed	0.353	0.709	**0.307**	**0.151**
No Retraining	0.267	0.625	0.143	0.036
Fixed Loss	0.178	0.472	0.099	0.028
No JPEG	**0.362**	0.728	0.254	0.083
No JPEG/Retraining	0.289	**0.740**	0.012	0.005
No Shifts	0.340	0.696	0.250	0.056
No Diagonal	0.189	0.281	0.125	0.060

Table 2: Ablation study of the method. **No JPEG**: pretraining was only done on uncompressed images. **No Retraining**: We directly use the pretrained network. **Fixed loss**: The target cannot be shifted to minimize the loss. **No Shifts**: the shifting JPEG described in Sec. 3.2 was not applied. **No Diagonal**: Detections were only made with the full pattern. **No Segmentation**: The score of each block is not maximized within each connected components.

5. Discussion

In this article, we have shown that positional and internal learning could be coupled to detect image forgeries as shifts in the image's demosaicing pattern. The self-supervised nature of positional learning makes it fit for internal learning, as labels can be directly obtained from the tested image, considering it is authentic. The main difficulty that could be expected to come with single-image fine-tuning comes from overfitting, especially on forged regions. While an overfitting network will detect all pixels' locations, and will thus fail to detect the forgery, it will not lead to a higher number of false positives. Overfitting is naturally limited by the small size of forgeries, combined with the fact that forgeries create evidence that contradict the rest of the image.

Our experiments show that our method detects demosaicing pattern shifts better than other demosaicing detection methods, and more generally beats the state of the art on the Korus dataset of uncompressed forged images.

Internal learning was performed with 15 iterations on each tested image. This number has been set heuristically, as results do not seem to improve much after that. In future work, obtaining an automatic stopping criterion would be desirable, to increase both the speed and detections.

We observed that demosaicing pattern detection is mostly undetected by more generic SOTA forensic algorithms, whereas our method specifically focuses on those. When trying to find forgeries, these methods yield complementary results and can thus work in parallel, not in competition. To this end, future work should focus on ways to interpret its results, to further limit its number of false detections and enable joint use with other methods.

References

[1] Irene Amerini, Rudy Becarelli, Roberto Caldelli, and Andrea Del Mastio. Splicing forgeries localization through the use of first digit features. In *2014 IEEE International Workshop on Information Forensics and Security (WIFS)*, pages 143–148. IEEE, 2014.

[2] Quentin Bammey, Rafael Grompone von Gioi, and Jean-Michel Morel. Automatic detection of demosaicing image artifacts and its use in tampering detection. In *2018 IEEE Conference on Multimedia Information Processing and Retrieval (MIPR)*, pages 424–429, April 2018.

[3] Quentin Bammey, Rafael Grompone von Gioi, and Jean-Michel Morel. An adaptive neural network for unsupervised mosaic consistency analysis in image forensics. In *IEEE/CVF Conference on Computer Vision and Pattern Recognition (CVPR)*, June 2020.

[4] Quentin Bammey, Rafael Grompone von Gioi, and Jean-Michel Morel. Image Forgeries Detection through Mosaic Analysis: the Intermediate Values Algorithm. *Image Processing On Line*, 11:317–343, 2021. https://doi.org/10.5201/ipol.2021.355.

[5] Quentin Bammey, Tina Nikoukhah, Marina Gardella, Rafael Grompone von Gioi, Miguel Colom, and Jean-Michel. Morel. Non-Semantic Evaluation of Image Forensics Tools: Methodology and Database. In *Proceedings of the IEEE/CVF Winter Conference on Applications of Computer Vision*, January 2022. https://arxiv.org/abs/2105.02700.

[6] Jawadul H Bappy, Amit K Roy-Chowdhury, Jason Bunk, Lakshmanan Nataraj, and BS Manjunath. Exploiting spatial structure for localizing manipulated image regions. In *Proceedings of the IEEE international conference on computer vision*, pages 4970–4979, 2017.

[7] Jawadul H Bappy, Cody Simons, Lakshmanan Nataraj, BS Manjunath, and Amit K Roy-Chowdhury. Hybrid lstm and encoder-decoder architecture for detection of image forgeries. *IEEE Transactions on Image Processing*, 2019.

[8] Belhassen Bayar and Matthew C Stamm. Constrained convolutional neural networks: A new approach towards general purpose image manipulation detection. *IEEE Transactions on Information Forensics and Security*, 13(11):2691–2706, 2018.

[9] Tiziano Bianchi, Alessia De Rosa, and Alessandro Piva. Improved dct coefficient analysis for forgery localization in jpeg images. In *2011 IEEE International Conference on Acoustics, Speech and Signal Processing (ICASSP)*, pages 2444–2447. IEEE, 2011.

[10] Davide Chicco. Ten quick tips for machine learning in computational biology. *BioData mining*, 10:35–35, Dec 2017.

[11] Davide Chicco and Giuseppe Jurman. The advantages of the matthews correlation coefficient (mcc) over f1 score and accuracy in binary classification evaluation. *BMC genomics*, 21(1):6–6, Jan 2020.

[12] Chang-Hee Choi, Jung-Ho Choi, and Heung-Kyu Lee. Cfa pattern identification of digital cameras using intermediate value counting. In *Proceedings of the Thirteenth ACM Multimedia Workshop on Multimedia and Security*, MM&Sec '11, pages 21–26, New York, NY, USA, 2011. ACM.

[13] Davide Cozzolino, Giovanni Poggi, and Luisa Verdoliva. Splicebuster: A new blind image splicing detector. In *2015 IEEE International Workshop on Information Forensics and Security (WIFS)*, pages 1–6. IEEE, 2015.

[14] Davide Cozzolino and Luisa Verdoliva. Noiseprint: a cnn-based camera model fingerprint. *IEEE Transactions on Information Forensics and Security*, 2019.

[15] Christophe Destruel, Vincent Itier, Olivier Strauss, and William Puech. Color noise-based feature for splicing detection and localization. In *2018 IEEE 20th International Workshop on Multimedia Signal Processing (MMSP)*, pages 1–6. IEEE, 2018.

[16] J. Duran and A. Buades. Self-similarity and spectral correlation adaptive algorithm for color demosaicking. *IEEE TIP*, 23(9):4031–4040, Sept 2014.

[17] J. Duran and A. Buades. A Demosaicking Algorithm with Adaptive Inter-Channel Correlation. *IPOL*, 5:311–327, 2015.

[18] Thibaud Ehret and Gabriele Facciolo. A Study of Two CNN Demosaicking Algorithms. *Image Processing On Line*, 9:220–230, 2019. https://doi.org/10.5201/ipol.2019.274.

[19] Pascal Getreuer. Gunturk-altunbasak-mersereau alternating projections image demosaicking. *Image Processing on Line*, 1:90–97, 2011.

[20] Pascal Getreuer. Zhang-wu directional lmmse image demosaicking. *Image Processing On Line*, 1:117–126, 2011.

[21] Pascal Getreuer. Image Demosaicking with Contour Stencils. *Image Processing On Line*, 2:22–34, 2012. https://doi.org/10.5201/ipol.2012.g-dwcs.

[22] Aurobrata Ghosh, Zheng Zhong, Terrance E Boult, and Maneesh Singh. Spliceradar: A learned method for blind image forensics. In *The IEEE Conference on Computer Vision and Pattern Recognition (CVPR) Workshops*, June 2019.

[23] Thomas Gloe and Rainer Böhme. The 'Dresden Image Database' for benchmarking digital image forensics. In *Proceedings of the 25th Symposium On Applied Computing (ACM SAC 2010)*, volume 2, pages 1585–1591, 2010.

[24] Edgar González Fernández, Ana Sandoval Orozco, Luis García Villalba, and Julio Hernandez-Castro. Digital image tamper detection technique based on spectrum analysis of cfa artifacts. *Sensors*, 18(9):2804, Aug 2018.

[25] Chuan Guo, Geoff Pleiss, Yu Sun, and Kilian Q Weinberger. On calibration of modern neural networks. In *International Conference on Machine Learning*, pages 1321–1330. PMLR, 2017.

[26] John F Hamilton Jr and James E Adams Jr. Adaptive color plan interpolation in single sensor color electronic camera, May 13 1997. US Patent 5,629,734.

[27] Chryssanthi Iakovidou, Markos Zampoglou, Symeon Papadopoulos, and Yiannis Kompatsiaris. Content-aware detection of jpeg grid inconsistencies for intuitive image forensics. *Journal of Visual Communication and Image Representation*, 54:155–170, 2018.

[28] Daniel Cavalcanti Jeronymo, Yuri Cassio Campbell Borges, and Leandro dos Santos Coelho. Image forgery detection by semi-automatic wavelet soft-thresholding with error level analysis. *Expert Systems with Applications*, 85:348–356, 2017.

[29] Thibaut Julliand, Vincent Nozick, and Hugues Talbot. Automated image splicing detection from noise estimation in raw images. 2015.

[30] Yongzhen Ke, Qiang Zhang, Weidong Min, and Shuguang Zhang. Detecting image forgery based on noise estimation. *International Journal of Multimedia and Ubiquitous Engineering*, 9(1):325–336, 2014.

[31] Daisuke Kiku, Yusuke Monno, Masayuki Tanaka, and Masatoshi Okutomi. Residual interpolation for color image demosaicking. In *2013 IEEE International Conference on Image Processing*, pages 2304–2308. IEEE, 2013.

[32] Daisuke Kiku, Yusuke Monno, Masayuki Tanaka, and Masatoshi Okutomi. Minimized-laplacian residual interpolation for color image demosaicking. In *Digital Photography X*, volume 9023, page 90230L. International Society for Optics and Photonics, 2014.

[33] Diederik P Kingma and Jimmy Ba. Adam: A method for stochastic optimization. *arXiv preprint arXiv:1412.6980*, 2014.

[34] Matthias Kirchner. Efficient estimation of CFA pattern configuration in digital camera images. In *Media Forensics and Security*, 2010.

[35] Paweł Korus. Digital image integrity–a survey of protection and verification techniques. *Digital Signal Processing*, 71:1–26, 2017.

[36] P. Korus and J. Huang. Evaluation of random field models in multi-modal unsupervised tampering localization. In *Proc. of IEEE Int. Workshop on Inf. Forensics and Security*, 2016.

[37] P. Korus and J. Huang. Multi-scale analysis strategies in prnu-based tampering localization. *IEEE Trans. on Information Forensics and Security*, 2017.

[38] Alexander Krull, Tim-Oliver Buchholz, and Florian Jug. Noise2void-learning denoising from single noisy images. In *Proceedings of the IEEE Conference on Computer Vision and Pattern Recognition*, pages 2129–2137, 2019.

[39] Weihai Li, Yuan Yuan, and Nenghai Yu. Passive detection of doctored jpeg image via block artifact grid extraction. *Signal Processing*, 89(9):1821–1829, 2009.

[40] Zhouchen Lin, Junfeng He, Xiaoou Tang, and Chi-Keung Tang. Fast, automatic and fine-grained tampered jpeg image detection via dct coefficient analysis. *Pattern Recognition*, 42(11):2492–2501, 2009.

[41] Bo Liu and Chi-Man Pun. Splicing forgery exposure in digital image by detecting noise discrepancies. *International Journal of Computer and Communication Engineering*, 4(1):33, 2015.

[42] Babak Mahdian and Stanislav Saic. Using noise inconsistencies for blind image forensics. *Image and Vision Computing*, 27(10):1497–1503, 2009.

[43] Owen Mayer, Belhassen Bayar, and Matthew C Stamm. Learning unified deep-features for multiple forensic tasks. In *Proceedings of the 6th ACM Workshop on Information Hiding and Multimedia Security*, pages 79–84. ACM, 2018.

[44] Owen Mayer and Matthew C Stamm. Learned forensic source similarity for unknown camera models. In *2018 IEEE International Conference on Acoustics, Speech and Signal Processing (ICASSP)*, pages 2012–2016. IEEE, 2018.

[45] O. Mayer and M. C. Stamm. Forensic similarity for digital images. *IEEE Transactions on Information Forensics and Security*, 2019.

[46] Yusuke Monno, Daisuke Kiku, Masayuki Tanaka, and Masatoshi Okutomi. Adaptive residual interpolation for color image demosaicking. In *2015 IEEE International Conference on Image Processing (ICIP)*, pages 3861–3865. IEEE, 2015.

[47] Tina Nikoukhah, Jérémy Anger, Thibaud Ehret, Miguel Colom, Jean-Michel Morel, and Rafael Grompone von Gioi. Jpeg grid detection based on the number of dct zeros and its application to automatic and localized forgery detection. In *Proceedings of the IEEE Conference on Computer Vision and Pattern Recognition Workshops*, pages 110–118, 2019.

[48] Xunyu Pan, Xing Zhang, and Siwei Lyu. Exposing image splicing with inconsistent local noise variances. In *2012 IEEE International Conference on Computational Photography (ICCP)*, pages 1–10. IEEE, 2012.

[49] Ibrahim Pekkucuksen and Yucel Altunbasak. Gradient based threshold free color filter array interpolation. In *2010 IEEE International Conference on Image Processing*, pages 137–140. IEEE, 2010.

[50] A.C. Popescu and H. Farid. Exposing digital forgeries in color filter array interpolated images. *Trans. Sig. Proc.*, 53(10):3948–3959, Oct. 2005.

[51] Alin C Popescu and Hany Farid. Statistical tools for digital forensics. In *Information Hiding*, pages 128–147. Springer, 2004.

[52] Yuhui Quan, Mingqin Chen, Tongyao Pang, and Hui Ji. Self2self with dropout: Learning self-supervised denoising from single image. In *IEEE/CVF Conference on Computer Vision and Pattern Recognition (CVPR)*, June 2020.

[53] M Ali Qureshi and M Deriche. A review on copy move image forgery detection techniques. In *2014 IEEE 11th International Multi-Conference on Systems, Signals & Devices (SSD14)*, pages 1–5. IEEE, 2014.

[54] Hyun Jun Shin, Jong Ju Jeon, and Il Kyu Eom. Color filter array pattern identification using variance of color difference image. *Journal of Electronic Imaging*, 26(4):1 – 12, 2017.

[55] Runjie Tan, Kai Zhang, Wangmeng Zuo, and Lei Zhang. Color image demosaicking via deep residual learning. In *2017 IEEE International Conference on Multimedia and Expo (ICME)*, pages 793–798. IEEE, 2017.

[56] Savita Walia and Mandeep Kaur. Forgery detection using noise inconsistency: A review. *International Journal of Computer Science and Information Technologies*, 5(6):7618–7622, 2014.

[57] Heng Yao, Shuozhong Wang, Xinpeng Zhang, Chuan Qin, and Jinwei Wang. Detecting image splicing based on noise level inconsistency. *Multimedia Tools and Applications*, 76(10):12457–12479, 2017.

[58] Shuiming Ye, Qibin Sun, and Ee-Chien Chang. Detecting digital image forgeries by measuring inconsistencies of

blocking artifact. In *2007 IEEE International Conference on Multimedia and Expo*, pages 12–15. Ieee, 2007.

[59] Wael AbdAlmageed Yue Wu and Premkumar Natarajan. Mantra-net: Manipulation tracing network for detection and localization of image forgerieswith anomalous features. 2019.

[60] Hui Zeng, Yifeng Zhan, Xiangui Kang, and Xiaodan Lin. Image splicing localization using pca-based noise level estimation. *Multimedia Tools and Applications*, 76(4):4783–4799, 2017.

[61] Kai Zhang, Wangmeng Zuo, Yunjin Chen, Deyu Meng, and Lei Zhang. Beyond a gaussian denoiser: Residual learning of deep cnn for image denoising. *IEEE transactions on image processing*, 26(7):3142–3155, 2017.